ELSEVIER

Marine Chemistry 53 (1996) 131–145

MARINE CHEMISTRY

Modeling, measurements, and satellite remote sensing of biologically active constituents in coastal waters

Dana R. Kester *, Mary F. Fox, Andrea Magnuson

Graduate School of Oceanography, University of Rhode Island, Narragansett, RI 02882, USA

Received 1 April 1994; accepted 29 June 1995

Abstract

We examine ways of addressing coastal environmental quality concerns through the use of modeling, measurements, and in the future, satellite remote sensing. In a summary of historical trace-metal concentrations in the waters of Narragansett Bay, we partitioned the estuary into sectors that reflect the morphology of the Bay and the transition between freshwater inputs and offshore coastal waters. We constructed a 24-box two-layer model of the Bay. A convenient summary of the chemical variations in the Bay was provided by a schematic diagram which for a constituent such as copper or other metals displays the average concentration, the range, the standard deviation, and the number of observations in our database for each sector. This diagram shows the spatial gradients through the Bay and the variability within a sector. Using a simple two-layer box model with seven transport terms we computed the physical exchanges between boxes using freshwater input and salinity data. The box model approach was applied in greater detail to the upper portion of Narragansett Bay to provide transport terms for use in an oxygen water quality evaluation. A digital bathymetric map of the estuary was compiled to enable volume-weighted calculations of physical and chemical properties. A seasonally variable data set was available to determine the effects of summer/winter and high-/low-runoff conditions on the oxygen concentrations of the waters. Using the freshwater input rates and the observed salinity distribution in the estuary we calculated the transport of waters between boxes and the residence times of water within each box. The model was applied to oxygen concentrations in the estuary incorporating estimates of the effects of air–sea exchange, of sediment oxidation demand, of photosynthetic production and respiratory consumption, and of biochemical oxygen demand from sewage treatment effluents. The model provides a basis to estimate the relative importance of various processes that may cause low oxygen conditions in the waters.

An investigation of oxygen variations in coastal waters was conducted with an Endeco/YSI rapid-pulse dissolved oxygen electrode. A 30-day time series was obtained at a depth of 1–2 m in Narragansett Bay. Measurements of oxygen, temperature, and salinity were obtained every 30 min during October 1993. Fourier analyses were used to determine the frequencies in the oxygen, temperature, and meteorological (wind speed and sunlight levels) variables. There was a strong diel signal in oxygen with smaller amplitude variations at the semidiurnal tidal frequency and a large amplitude variation with a period of 3–5 days. High temporal resolution data are needed to detect the events in coastal waters that result in substantial chemical variations of biologically active constituents such as oxygen.

In anticipation of possible applications of the next generation ocean color satellite sensor, SeaWiFS, we have been examining the historical CZCS data from the region off the northeastern U.S.A. We have worked with both the 4-km and the 1-km horizontal resolution CZCS data. The scales of variability that are evident are in the range of 5–50 km. For quantitative use of the ocean color data attention must be given to spatial variations in the atmospheric attenuation of the

* Corresponding author.

PII S0304-4203(96)00019-9

visible radiation, and to the separation of chlorophyll, suspended matter, and possibly blue-absorbing organic matter in the ocean color signal.

1. Introduction

Coastal waters throughout much of the world are being affected by anthropogenic inputs of nutrient elements (e.g., N, P, and Si), of organic matter that undergoes bacterial degradation consuming dissolved oxygen and releasing nutrients, of pathogenic organisms, of potentially toxic trace metals, and of natural and synthetic organic compounds (e.g., petroleum hydrocarbons, pesticides, PCBs). These inputs are related directly to increases in human population density, agriculture, and industrial development in coastal regions. A common concern in many areas with substantial coastal urban development is eutrophication, in which the balance of nutrients is altered leading to harmful algal blooms and excessive production of nuisance photosynthetic organisms. In some regions there are episodes of anoxia in which dissolved oxygen is totally depleted leading to massive kills of important living marine resources.

The objective of this paper is to examine ways of addressing coastal environmental quality concerns through the use of modeling, measurements, and in the future, satellite remote sensing. We will present the results of a series of investigations conducted in recent years in Narragansett Bay, Rhode Island. This work requires the integration of knowledge concerning chemical, physical, and biological processes in coastal regions. A major concern is to adequately resolve the time and space scales on which natural processes and anthropogenic effects occur. While the specific results that we present are derived from a particular estuary, the methodologies used should be applicable to estuarine and coastal systems in general.

This paper summarizes five investigations. One is an examination of dissolved copper concentrations in Narragansett Bay based on a compilation of about ten years of analytical measurements by several investigators (Bender et al., 1989). The second is the formulation of a simple box model for transport processes in Narragansett Bay which can be used to examine the non-conservative behavior of a reactive pollutant such as copper. Third is a more extensive box model analysis of the upper portion of Narragansett Bay where there are major water quality concerns associated with extensive urban and industrial development. These box model results have been applied to a dissolved oxygen model (Dettmann et al., 1992). Fourth are some recent results we obtained during an evaluation of a newly developed rapid-pulse oxygen sensor for marine environmental use. Finally, we present some results from an examination of Coastal Zone Color Scanner chlorophyll images for northeastern U.S.A. waters in order to define the horizontal scales of variability of biologically important processes.

2. Copper in Narragansett Bay

Narragansett Bay is one of the major estuaries in the northeastern U.S.A. It is a drowned valley with a series of islands separating the Bay into north–south-trending channels. The Bay receives freshwater input from several relatively small rivers and it is tidally flushed with waters from Rhode Island Sound. The head of Narragansett Bay is the major urban region of the State of Rhode Island with the cities of Providence, Pawtucket, East Providence, and Cranston comprising $> 50\%$ of the State's nearly one million people, and much of its industry. As part of an historical summary of the environmental quality of Narragansett Bay, Bender et al. (1989) compiled a database of all the analyses of trace metals in the waters, sediments, and marine organisms of the Bay that were judged to be reliable. In this section we present a summary of copper in Bay waters and illustrate a box model that provides estimates of copper fluxes and residence times in various portions of the Bay.

Many investigators have found it useful to partition the Bay into a set of sectors which are determined by the major morphological features of the Bay. These earlier studies of the Bay tended to neglect the potential importance of areas known as Mount Hope Bay, the Seekonk River, and the Sakonnet River. The term "river" applied to the latter two areas is a misnomer, because they have only weak

net flow, with most of the flow being tidal, and they are principally seawater rather than fresh water. We will henceforth refer to these areas as estuaries. We extended the Bay segmentation approach of previous workers to include the Seekonk estuary, Mount Hope Bay, Sakonnet estuary, and the adjacent Rhode Island Sound (Fig. 1). To maintain consistency with other studies we retained the sector numbering of regions 1–8 of the Bay and added the additional four regions as 9–12. This segmentation scheme lends itself to the formulation of a box model of Narragansett Bay, which can be useful in identifying important features of the system. It will be convenient to represent the 12 regions in schematic form (Fig. 1).

After compiling the chemical database we constructed a simple statistical summary of the major properties of the Bay. Salinity provides an example of this summary (Fig. 2). For each sector and each property we show the average ± the standard deviation (the number of observations), and the minimum and the maximum values in the database. Reading horizontally across the ± symbol in a sector shows the characteristic value and its variation as well as how many observations are available. Reading vertically through the ± symbol shows the range of values in the database. Examining the minimum and maximum values among various sectors was helpful in identifying outliers which were not consistent with the overall pattern. Fig. 2 shows several important features about Narragansett Bay.

Most of the estuarine salinity gradient occurs in the Seekonk estuary. This is a region of the Bay where a salt-wedge occurs, and where one can find the low salinities associated with flocculation processes. The salinities are slightly lower in the West Passage of the Bay (sectors 3–5) than in the East Passage (sectors 6–8). There is a fairly frequently observed salinity reversal in the trend between sectors 2, 3, and 4. While there is a source of freshwater input into sector 3 (the Hunt River) its flow does not seem to be large enough to cause the observed

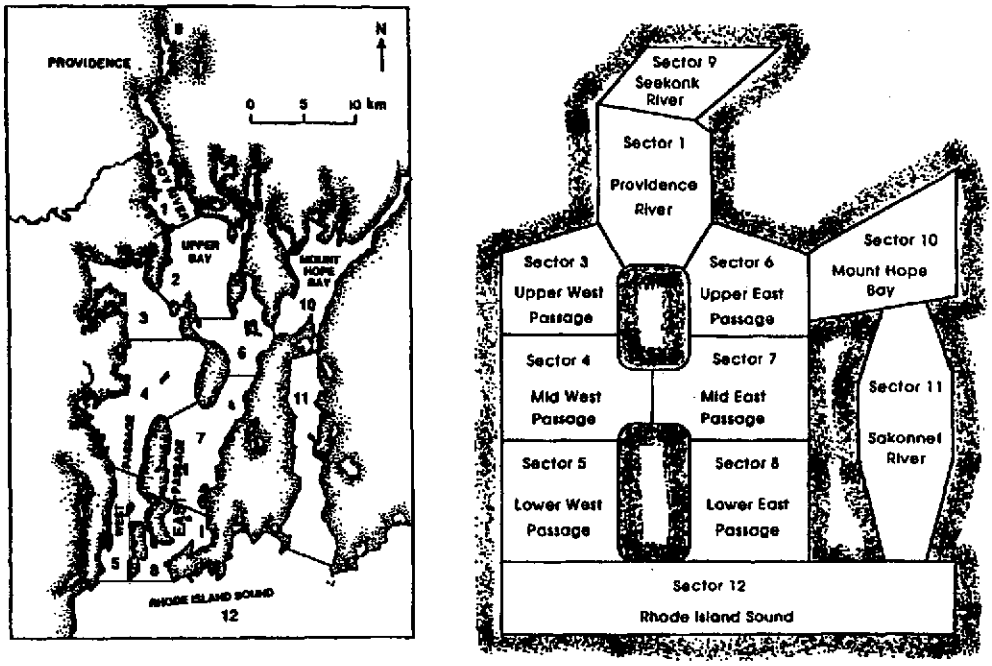

Fig. 1. Map of Narragansett Bay, Rhode Island, U.S.A., with 12 sectors identified (*left*), and schematic diagram of the 12 sectors of the Bay (*right*).

dilution in salinity. We have speculated that the lower salinity in this region could be an indication of groundwater input to the Bay. Sector 3 is the region with the fewest observations in our database; more extensive sampling of this sector should be done to determine the significance of the low salinities. The salinity difference between East and West Passages may be due to freshwater input in sector 3 or due to a greater net inflow of Rhode Island Sound seawater up the East Passage and net outflow of estuarine waters down the West Passage in response to tidal flows, wind-driven circulation, and Bay morphology. The salinity patterns among the 12 sectors are virtually the same whether one looks at the average, the minimum, or the maximum values.

The sector summary of the Bay is also useful for examining the variations in dissolved copper (Fig.

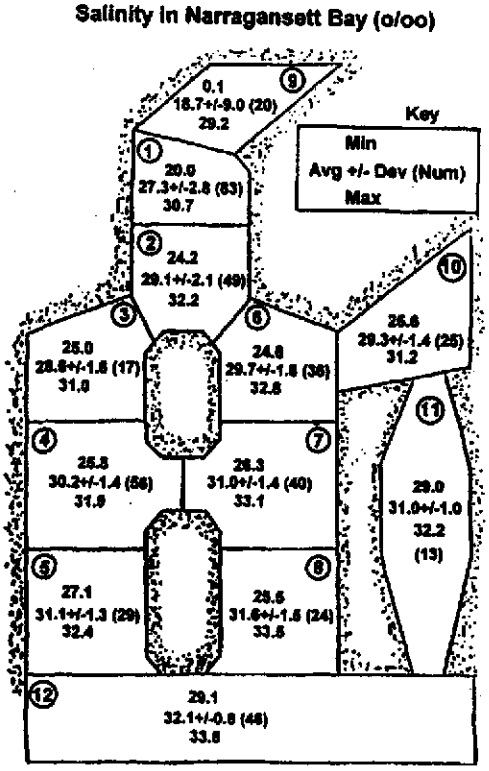

Fig. 2. Summary of the salinity database for Narragansett Bay with the average, standard deviation, minimum, maximum, and number of observations for each sector.

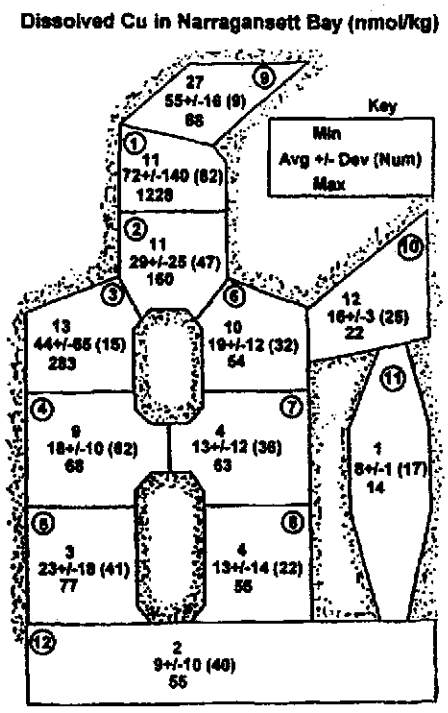

Fig. 3. Summary of the dissolved copper concentrations in Narragansett Bay with the average, standard deviation, minimum, maximum, and number of observations for each sector.

3). There is a general gradient of Cu down the Bay. There is also a difference in East and West Passages consistent with the salinity difference, in that the lower values in the East Passage reflect more saline–low Cu Rhode Island Sound water, and the higher values of the West Passage reflect more upper Bay waters which have high Cu concentrations. The extreme maximum Cu in sector 1 might be considered an outlier, but we have documentation that this sample was taken from the "boil" above the Providence sewage treatment facility effluent discharge (copper concentrations in the effluent prior to discharge from the pipe are in the range of 5,000–15,000 nmol/kg). The high maximum Cu in sector 3 also raises questions about whether it is an outlier or whether there is a significant source of Cu in region 3. This value (283 nmol/kg) was from a surface sample of relatively low salinity (27.6‰), and the next highest Cu concentration observed in sector 3

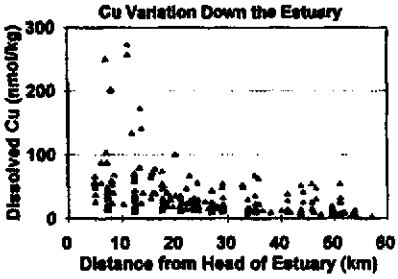

Fig. 4. Dissolved copper concentration vs. distance down the Bay.

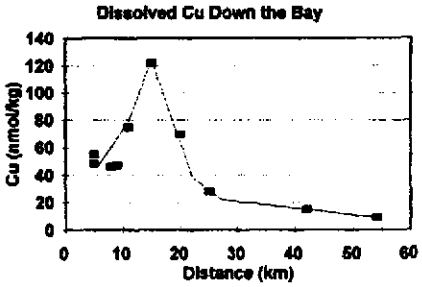

Fig. 6. Dissolved copper concentration calculated as the average copper concentration in each 2‰ salinity bin from 0–34‰ plotted vs. the average distance down the Bay for each salinity bin. This procedure removes the scatter in Fig. 4 that is due to the salinity variability seen in Fig. 5.

was 55 nmol/kg at the same location from a depth of 8 m. These two high values are from the same analyst in work done in 1977. All the other samples from sector 3 during the period 1978–1986 gave Cu values in the range of 24–33 nmol/kg. We excluded the two high Cu values in sector 3 from subsequent analyses of the data.

One objective in compiling this database was to describe the down-bay gradient in pollutant metals such as Cu. A direct plot of dissolved Cu concentration with distance down the estuary shows a great deal of scatter (Fig. 4). Unlike many other estuaries where rivers bring in the major concentrations of pollutants, in Narragansett Bay a major input of Cu has been the effluent of the Providence sewage treatment facility. The high Cu concentrations (> 150 nmol/kg) are associated with this source. One of the causes for the large amount of scatter in Fig. 4 is shown in Fig. 5, which is a similar down-bay plot of salinity. The difference in salinity between surface and deep waters, and the tidal excursion of high-salinity waters up the Bay means that you may find water with salinities between 25‰ and 30‰ over much of the length of the Bay. We removed the effect of salinity variations from the down-bay Cu gradient by sorting the data according to salinity and then averaging the dissolved Cu concentration, and the distance down-bay in 2‰ salinity intervals from 0 to 34‰. The resulting Cu gradient is shown in Fig. 6. Waters upstream of the sewage treatment effluent discharge have Cu concentrations of ~ 50 nmol/kg, and the high values associated with the effluent discharge decrease substantially within 15 km of the discharge point, indicating significant removal of Cu from the water column and most likely incorporation into the sediments. The behavior of Cu in this system can be seem by separating the surface waters (0–3 m) and deep waters (> 3 m), calculating the salinity-binned average metal concentrations, and plotting these averages against the salinity (Fig. 4). Dissolved Cu, Ni, and Pb all show similar plots vs. salinity, indicating that the sewage treatment effluent is a significant source of these three metals. Cadmium and silver, in contrast, show linear variations with salinity, and no unusually high values in the vicinity of 25‰ salinity. The most significant inputs of Cd and Ag are with the freshwater inputs to the upper Bay.

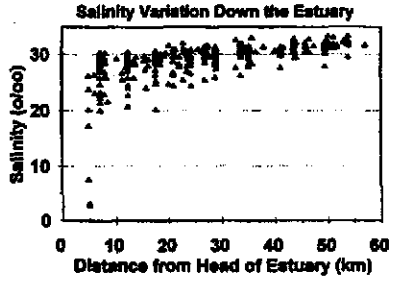

Fig. 5. Salinity vs. distance down the Bay.

3. A box model consideration of Narragansett Bay

The segmentation of this estuarine system leads to the formulation of a box model to describe the transport of waters and pollutants through the estu-

ary. A simple box model was formulated in which each sector is divided into a surface box and a deep box, and six transport terms are used to describe the net estuarine circulation (Fig. 7). By knowing the salinities in each box and the freshwater inputs (FWs) to each surface box it is possible to calculate the seawater transport terms (in units such as $m^3\ s^{-1}$) which is required to maintain the observed salinities. Fig. 7 shows the six transports for the ith sector in relation to its adjacent sectors. T_1 and T_2 are the net estuarine outflow in the surface; T_3 and T_4 are the net inflow of offshore water at depth, T_5 and T_6 allow for vertical mixing and upwelling between the surface and deep boxes. To simplify the application of this model the Narragansett Bay, we combined the corresponding sectors of the East and West Passages (3 and 6, 4 and 7, 5 and 8). The effects of sector 10 were included as a tributary input to the main portion of Narragansett Bay, but it is not shown as an additional box in the model results. For each sector there are four conservation equations that must be satisfied: conservation of volume in the surface box and in the deep box, and conservation of salt in the each of these two boxes. It might appear that this system is under-determined with six transports and only four equations, but for each sector there are actually only four new transports, and the equations

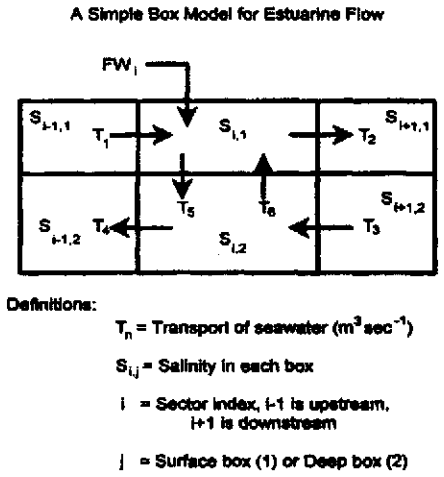

Fig. 7. Schematic of the simple box model for estuarine transport of waters based on salinity and freshwater input (FW).

Box	Property	Sector 1	2	3	4	5	6	7
Surface	Cu–nmol/kg	54.3	75.3	26.2	25.4	19.75	16.1	12.1
	Volume–$10^6 m^3$	4.35	65.4	149	171	577	140	
	Flux In–mol/day	239	1023	3390	1950	3258	4430	
	Flux Out–mol/day	319	704	1707	2414	2175	3315	
	Res.Time–day	0.21	1.43	0.38	0.50	1.05	0.15	
Deep	Cu–nmol/kg	56.5	22	20.6	20.1	11.6	9.4	7.3
	Volume–$10^6 m^3$	4.65	32.6	138	184	463	529	
	Flux In–mol/day	90	816	1639	1694	2485	3484	
	Flux Out–mol/day	200	622	1625	1419	2100	3255	
	Res.Time–day	0.45	0.25	0.43	0.58	0.60	0.37	

Transports–m^3/s

T1	0	64	321	857	920	1248
T2	64	321	857	920	1248	2823
T3	37	278	812	847	1174	2749
T4	0	37	278	812	847	1174
T5	4	49	101	470	886	1258
T6	41	291	835	5	1213	2834

Fig. 8. Summary of the results of the box model calculations of dissolved copper in Narragansett Bay. The 12 sectors in Fig. 1 have been simplified by combining the corresponding sectors of the East and West Passages (3 + 6, 4 + 7, and 5 + 8), and by treating Mount Hope Bay (sector 10) as a tributary input. The sectors down the Bay have been renumbered in sequence from 1 at the head of the estuary to 7, which is Rhode Island Sound. The upper portion of the diagram give the Cu concentration and the flux of dissolved Cu in and out of each box. The residence time of dissolved Cu is also given in each box. The lower matrix gives the transports of water in $m^3\ s^{-1}$ required to balance the salinity and freshwater input for each sector.

can be solved. If one starts at the head of the estuary (sector 9 in our case), it is evident that T_1 and T_4 are both zero for the uppermost sector, and the four equations are solved for T_2, T_3, T_5, and T_6. In subsequent sectors the T_1 and T_4 are known from the T_2 and T_3 of the preceding sector.

The results of the box model including flux calculations for Cu are shown in Fig. 8. For this summary the sectors have been labelled sequentially from the head (#1) to the mouth (#7) of the estuary. Each sector has a surface and deep box, and we have shown the average observed dissolved Cu in each box, the volume of each box, and the fluxes of Cu in and out due to the six transport terms and the point source inputs to the surface boxes. We have also calculated the residence time of Cu in each box. The six transports for each sector required to balance the salinity distribution are shown in the matrix beneath the boxes. The way this model is computed there is no assurance that the flux of Cu in and out of a box will be equal. A greater flux in than out can indicate removal of Cu and incorporation into the sediments. A greater flux out than in could indicate a flux out of the sediments, but this could not be sustained for an indefinite period of time, or it could indicate a conversion of particulate Cu to dissolved Cu within the box. The deep boxes for most of the Bay show quite a good balance between fluxes in and out. The deep box of the uppermost sector is exporting about twice as much Cu as it receives. This sector is smaller in volume than the others and its lack of balance does not greatly perturb the rest of the system. The large sewage input of Cu occurs in the surface box of the second sector and the Cu–salinity plot indicated removal of Cu from these waters which is also reflected in the greater flux in than out for the second and third sectors. The lower three surface boxes of the estuary have fluxes in and out that are within ~75% of being in balance.

The residence times of dissolved copper in all boxes are less than those of the seawater. Table 1 gives the residence times of seawater in each box (the box volume divided by the total water flux in or out of the box), and it also gives the ratio of the Cu residence time to the seawater residence time. In many cases copper is turning over 3–4 times more quickly than would occur if the only process were flushing of the waters in the Bay. The smaller the ratio of these residence times, the more important is biogeochemical cycling of copper to its flux through a box.

Table 1
Comparison of the residence times of waters and of dissolved copper in the simplified six-sector box model of Narragansett Bay (the ratio of the Cu to water residence times is given also)

Box	Component	Sector					
		1	2	3	4	5	6
		Residence time (days)					
Surface	water	0.8	2.0	1.8	1.4	1.6	0.4
	Cu	0.2	1.4	0.4	0.5	1.0	0.2
	Cu/water	0.25	0.70	0.22	0.36	0.63	0.50
Deep	water	1.3	1.2	1.7	1.6	4.0	1.5
	Cu	0.4	0.2	0.4	0.6	0.6	0.4
	Cu/water	0.31	0.17	0.24	0.38	0.15	0.27

4. A water quality box model approach to upper Narragansett Bay

The summary of historical data on pollutant concentrations in Narragansett Bay described in the previous section and the occurrence of low oxygen concentrations in upper Bay subsurface waters during summer months led to increased attention being given to the upper Bay — primarily sectors 1, 2, and 9 in Fig. 1. This water quality modeling effort was described in detail in a report by Dettmann et al. (1992). We developed a detailed box model for the upper portions of Narragansett Bay where most of the freshwater input, most of the pollutant input, and most of the salinity gradient occurs. The box model provided tidally averaged volume transports through this portion of the estuary. The U.S. Environmental Protection Agency developed a FORTRAN-language Water Quality Analysis Simulation Program (WASP) for use on personal computers. This model contains a series of modules that can be assembled to meet the requirements of specific analyses. In this study we used the box model to derive transport terms that are needed by WASP, and we used Version 4.2 of the EUTRO (eutrophication) module to examine the dynamics of oxygen, nutrients, and phytoplankton.

Fig. 9 shows the segmentation of the upper Bay that was used in this analysis. Nine sectors were

defined with a tenth region serving as a boundary condition for the exchange of substances with the middle and lower portions of the Bay.

One of the limitations of the simple box model used in the previous section is that the transports reflect the net circulation of waters through the estuary. A better description of these transports is provided if one can distinguish between the longitudinal tidal exchange (which has a diffusive character over many tidal cycles) and the longitudinal net advective flow (which is driven by freshwater flow through the estuary and by salt entrainment in that flow). Hansen and Rattray (1965, 1966)) characterized these two components of circulation in terms of an estuarine parameter, ν. This parameter is defined as the ratio of the longitudinal tidal diffusive exchange to the total longitudinal transport. For estuaries in which tidal exchange is the major flushing process ν will approach unity, and for estuaries in which the freshwater estuarine circulation is the major flushing process ν will approach zero. Most systems will have some value of ν between 0 and 1. One problem in applying the use of ν to estuarine circulation has been the lack of a means to determine the value of ν unless one has a complete hydrodynamic model of the system which computes the tidal and the non-tidal components of the circulation. In the course of our box modeling in Narragansett Bay we discovered a way to calculate ν from salinity and freshwater flow data. This method was reported by Officer and Kester (1991).

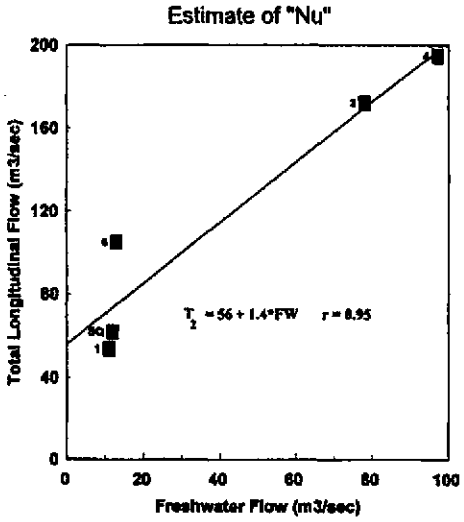

Fig. 10. Correlation between the total longitudinal flow of upper Bay sector 4 and the freshwater flow from five sets of data. The linear regression yields the intercept 56 m^3 s^{-1} which we take to be the tidal exchange, and the slope 1.4 which we take to be the entrainment factor for this sector.

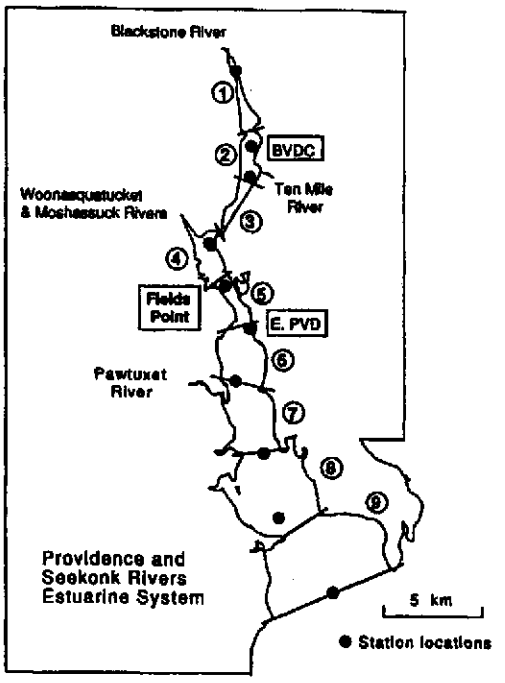

Fig. 9. Map of the upper portion of Narragansett Bay where the oxygen water quality model was developed.

In using the simple box model (Fig. 7) we found that a striking correlation exists between the transport flux out of a sector (T_2) and the freshwater flow through the box. If the simple model is used with salinity data obtained under a range of freshwater flow conditions, it is possible to calculate T_2 and plot its variation with FW. Fig. 10 shows such a plot for sector 4 of Fig. 9. In all cases we have examined such a plot shows a positive y-axis intercept which is the amount of longitudinal flushing at zero freshwater flow. The ratio of this intercept to T_2 gives an estimate of ν for a specific freshwater flow. This approach leads to a modification of the box model transports shown in Fig. 11, in which an additional

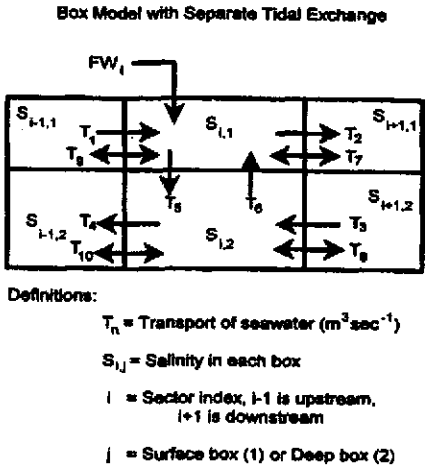

Fig. 11. An estuarine box model in which the tidal exchanges T_7-T_{10} are distinguished from the estuarine circulation transports.

bi-directional longitudinal transport is associated with tidal exchange. This additional term provides a means for a downstream surface box salinity to contribute to the salt flux of a surface box, and in the deep boxes for upstream boxes to contribute to the salt flux. The additional transports (T_7-T_{10}) were calculated.

Another interesting implication arises from Fig. 10. This type of plot was first demonstrated by Officer and Kester (1991) using a one-box model of Narragansett Bay. Pilson (1985) had computed the residence time of waters in the Bay from the average salinity of the Bay, the salinity of Rhode Island Sound, and the freshwater flow into the Bay over a 26-year period. The box model flushing rate vs. freshwater flow contained a fairly high degree of scatter, and Officer and Kester debated whether this should be represented by a linear, or a more complex, relationship. They chose to sketch a slightly sigmoid-shaped curve through the scattered data points to suggest that there might be hydraulically limiting flushing rates at very low and very high freshwater flows. In further tests of the total outflow vs. freshwater flow for subsections of Narragansett Bay such as used in this analysis, we have become more convinced that the observations are most consistent with a linear relationship over the flow rates for which we have data. The slope of this relationship (Fig. 10) corresponds to the entrainment ratio of seawater to fresh water in the estuarine circulation. For example, in the case of sector 4, shown in Fig. 10, the intercept is 56 $m^3\ s^{-1}$, which we take to be the flushing rate due to tidal mixing. The slope is 1.4 $m^3\ s^{-1}$ of total flow per $m^3\ s^{-1}$ of freshwater flow. Thus, each 1.0 $m^3\ s^{-1}$ of freshwater flow entrains 0.4 $m^3\ s^{-1}$ of seawater flow through the deep half of the estuarine circulation. This relationship between total flushing rate and freshwater flow merits examination in other estuarine systems. The slope and intercept of the relationship should be a characteristic parameter of the estuarine tidal mixing and estuarine circulation of each system.

A considerable amount of data processing was needed to implement this box model. The observational data that were available consisted of seven sets of measurements at the ten stations shown in Fig. 9. These data sets were obtained by Doering et al. (1988a,b) at various times during the year to determine the variations in properties under different freshwater flow rates and seasonal factors. Two sets of samples were collected at each observation period: one set at high tide and one set at low tide. Our model was designed to approximate tidally-averaged steady-state conditions. For these calculations we needed to compute box-volume weighted averages of various properties (salinity, temperature, oxygen, nutrients, metals, etc.). We also needed to know surface and cross-sectional areas for some of the box model calculations.

We obtained high-resolution digitized shoreline and bathymetry data for the estuary from U.S. Geological Survey (USGS) and U.S. National Oceanic and Atmospheric Administration (NOAA) data sets. These data sets had to be reconciled, because there were some registration problems with depth values appearing on land probably due to the interpolation/extrapolation procedures used in gridding the NOAA bathymetry. We also noted that the reference level for the shoreline differs from the reference level for depths in the marine environment. The USGS and NOAA define the shoreline to be mean high water, but depths are referenced to mean low water. The difference of these two elevations in the region of Fig. 9 is 1.4 m, which represents a significant volume, especially in the Seekonk estuary. We placed the shoreline and bathymetry on a consistent reference level by defining the shoreline

to be an elevation of + 1.4 m, and assigning negative values to all depths within the estuary. A commercially available microcomputer program (SURFER, Golden Software, Golden, Colorado, U.S.A.) was used to grid the shoreline and depth data, to generate contour maps, and to calculate the volume of the estuary between various depth intervals. This software was also able to calculate surface areas for specific elevations and vertical cross-section areas between the segments in our box model.

Salinity data from the estuary along with freshwater flow data into the estuary are the basis for calculating the physical transport terms in the box model. We used SURFER to grid (interpolate and extrapolate) the observed salinity values (at several depths from 10 stations) into uniformly spaced values every 0.5 m vertically and 0.5 km horizontally down the axis of the estuary. Nearly all observations from this estuary have been taken down the deepest axis of the estuary, which is a shipping channel dredged to a depth of ~ 13 m. Only rarely have investigators examined the gradients across this estuary. In those cases where there are data on the cross-estuary gradients in salinity, they are very small compared with the down-estuary gradients. For our model we assumed that salinity was uniform across the estuary.

The high-tide and low-tide salinity data sets were gridded and matched up with the volumes computed for each 0.5 m by 0.5 km element from the digital bathymetry and shoreline data. Since the observed salinity values are in terms of depths relative to the seawater surface (and this surface varies by 1.4 m from high to low tide) the two salinity data sets were shifted vertically by the tidal amplitude. The volume-weighted tidally-averaged salinity was then calculated for each box in the model. The boundary between the surface box and the deep box in each sector was selected, based on the halocline which ranged from 1.5 m in the upper portion of the estuary to 3.0 m in the lower portion (these depths are relative to mean low water). The salinity values and freshwater flows, along with the estimates of the ν parameter from the T_2–FW correlations for each sector (Fig. 10), were used to compute box model transports that balanced total volume and salt. These transports varied, of course, for each of the seven periods when field data were obtained.

The box model transports were used as inputs to the EUTRO module of WASP. This module allows the user to select the level of complexity with which the physical, chemical and biological processes are to be modeled. We used Level 3 complexity which includes: air–sea O_2 exchange, phytoplankton photosynthesis and respiration, reactive organic carbon oxidation, nitrification, organic nitrogen oxidation, and sediment oxygen demand. Level 3 does not attempt to model phytoplankton abundance from nutrient concentrations, light, and other variables. EUTRO contains algorithms for the various biogeochemical processes, and the user inputs rate constants appropriate to the system being modeled, physical transports, and boundary conditions. The model then calculates the resulting concentrations of a variable such as dissolved oxygen. The boundary conditions that were needed for this estuary included the flow and chemical compositions of river inputs and of point source anthropogenic inputs (primarily sewage treatment facility discharges), and the concentrations of variables at the downstream end of the estuary.

One observational data set obtained in September 1989 (Doering et al., 1989) was used to calibrate the EUTRO model. The calibration consisted of selecting specific values of rate constants for the various processes affecting oxygen that were within the range of rates observed in this or similar estuaries. The model was able to account for oxygen concentrations in nearly all boxes from the calibration data set. The model was then applied to other data sets in which the only changes were to the boundary conditions at the time of the measurements. Fig. 12 shows surface and deep box oxygen concentrations down the estuary computed from the model and observed in the Spray 1 dataset (October 1986). The agreement in absolute magnitude and trend is quite good.

One value of a model such as this is that it allows one to examine the sensitivity of oxygen concentrations to specific terms in the model. This model, its calibration and validation, and an exploration of its sensitivity to various processes was presented in detail by Dettmann et al. (1992). In this estuary sediment oxygen demand results in a ~ 10% reduction in oxygen concentrations. The model was surprisingly insensitive to the biological oxygen demand (BOD) from sewage treatment facilities, but

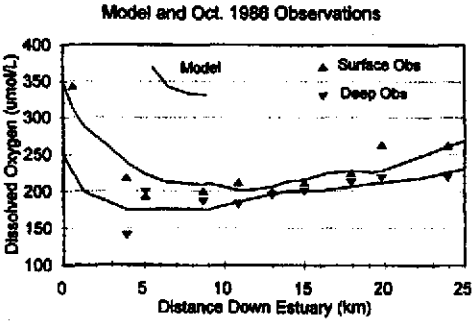

Fig. 12. Comparison of the WASP model oxygen concentrations in the surface and deep boxes with the values observed in October 1986. The model parameters were not adjusted to fit these observations. The model parameters were set in relationship to a separate data set obtained in September 1989.

the nutrients associated with this effluent stimulate phytoplankton production which then leads to oxygen depletion. Variations in the air–sea gas exchange rate had a small effect (< 10%) on the surface box oxygen concentrations, and this led to no significant effect on the deep box oxygen concentrations.

5. High-resolution oxygen time-series

An inherent limitation with many investigations in coastal waters is that the time and space scales of natural and anthropogenic changes are under-sampled. To overcome this limitation we must develop new methods of sampling and measurements which will more fully resolve the variations that exist. These methods will require automated and autonomous instruments for a range of chemical, physical, and biological properties. We have begun to evaluate the use of such methods for time-series measurements of dissolved oxygen, along with temperature and salinity. During the latter part of 1993 we performed an evaluation of a newly developed instrument by YSI, Inc. This instrument was a YSI 6000, which consisted of a rapid-pulse oxygen sensor, a temperature sensor, and a conductivity sensor. The YSI 6000 is a self-contained data logging instrument which operates on eight alkaline C cells. It stores the readings internally, and it can be connected to a personal computer via an RS-232 port for data transfer and instrument programmability.

The objectives of our evaluation were: (1) to determine the sensitivity of the sensors to natural variations in coastal waters near the entrance of Narragansett Bay; (2) determine the stability of the sensors for deployments up to 30 days; (3) evaluate a calibration protocol for the instrument; (4) examine possible problems related to bio-fouling of the sensors; and (5) examine the response characteristics of the sensors under laboratory conditions. Our evaluations consisted of two modes of operation. The YSI 6000 was suspended from the Graduate School of Oceanography (GSO) dock from October 1 through October 30, 1993. The instrument was also used in a series of laboratory calibration experiments.

The YSI 6000 was suspended from the outer-most portion of the GSO dock where the water depth is ~7 m. The sensors were ~1 m beneath the sea surface at low tide, and 2 m beneath the surface at high tide. For the laboratory calibration tests we wanted to compare the air-calibration protocol recommended by YSI with aqueous phase calibrations using Winkler oxygen titrations. We also wanted to be able to evaluate any flow rate dependence of the oxygen sensor. Finally, we wanted to examine the response time when the sensors are subjected to a step function change in oxygen, salinity, and temperature. YSI recommends a one-point air calibration for the rapid-pulse oxygen sensor.

We found the rapid-pulse oxygen sensor to be remarkably stable over a 4-month period. An air calibration was performed in August 1993 and it was checked at various times during our experiments through early December 1993. The air calibration value did not change by more than 2.5% and no long-term drift was observed over the four months. The response of the oxygen sensor to a step function change in seawater oxygen saturation from 101% to 39% was complete within 3 min (Kester and Magnuson, 1994).

Fig. 13 shows the 30-day time-series of salinity, temperature, and oxygen from the GSO dock (which is located on the west shore at the middle of sector 5 in Fig. 1). The instrument was programmed to warm up for 50 s and take a reading once every minute. The salinity values were between 30‰ and 31‰; these values were scaled by dividing the salinity by 2.0 and adding 2.0, in order to plot them on the same numerical scale as temperature. The salinity digitiza-

tion of 0.1‰ is too coarse to provide useful salinity variations in this environment where the range of variations is < 1‰. The temperature during the month decreased, reflecting the seasonal cooling of the waters which is typical of this time of the year. The 0.1°C digitization of the temperature signal by the YSI 6000 is evident in this record. The cooling rate varies with meteorological conditions (such as air temperature changes, wind speed, and storms) and possibly due to variations in tidal range. The degree of oxygen saturation shows a photosynthetic bloom from October 5–9 followed by a crash and then a smaller event near the end of the month. The temperature and oxygen record show two dominant periods of variation. The major amplitude signal has a diel frequency in which the waters are warmed during the day-time and oxygen is produced photosynthetically. The smaller amplitude variation is tidal: each low tide is associated with slightly warmer and higher oxygen saturation conditions. We believe that this tidal signal is mainly due to the tidal excursion that exchanges waters at this site between the offshore regions of Rhode Island Sound and the mid-Bay waters. The vertical gradients of temperature and oxygen in the upper 1–2 m of the water column were too slight to account for the tidal signal. The oxygen saturation values show very large diel changes associated with the phytoplankton photosynthesis bloom during October 6–8.

The predominant frequencies of variation of the oxygen time-series have been determined by using a Fourier transform (Fig. 14) of the oxygen saturation

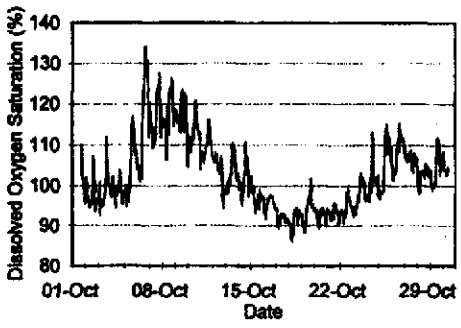

Fig. 13. Time-series of oxygen variations near the mouth of Narragansett Bay based on readings every 30 min from a YSI rapid-pulse dissolved oxygen electrode. These measurements were made in 1993.

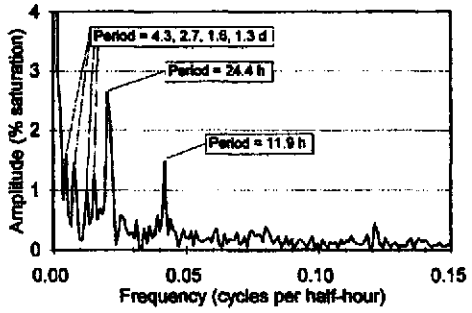

Fig. 14. Fourier transform of the oxygen time-series showing the characteristic frequencies corresponding to the semi-diurnal tide, the diel cycle, and events with periods in the range of 1.3–4.3 days, which appear to be mainly meteorological. The average % saturation for the month of October (102.7%) was subtracted from the observations before the transform was computed.

minus the mean for the series (102.7%). A large amplitude signal is present at ~21 days, which is the period of the photosynthesis blooms. A longer record would be needed to establish the persistence of this frequency. The remaining largest amplitude frequencies occur at values corresponding to periods of 4.3, 2.7, 1.6, and 1.3 days, and to 24.4 and 11.9 h. The 11.9-h period is close to the semi-diurnal tidal period; the 24.4-h period represents the diel variation in oxygen due to photosynthesis and respiration. The ~1.5–4.5-day periods are driven most likely by meteorological factors such as the amount of cloud cover (sunlight) and the effects of wind. In this region weather patterns tend to move through with a 3-day period.

To illustrate the time scales of oxygen variability we have digitally filtered the data in Fig. 14 to isolate specific frequency ranges. Fig. 15 shows the variations associated with periods longer than the diel cycle; the mean was added back into this signal to show the departure from equilibrium with the atmosphere. This signal represents the main bloom–crash cycle and the meteorologically driven variations in oxygen. Fig. 16 shows the data processed by a band pass filter which eliminates periods shorter than the diel and longer than 2.2 days. This treatment of the data shows the variations in amplitude of the diel signal. During the bloom conditions (October 6–9) the amplitude is quite large. During a cloudy period (October 15–20) the amplitude is small. The

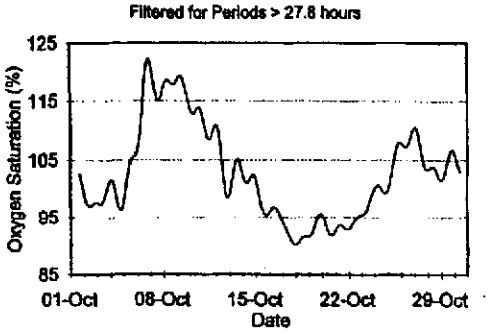

Fig. 15. The variability of oxygen saturation on periods longer than the diel period. The data in Fig. 13 were digitally filtered to remove the variations that are diel and shorter in duration.

high-frequency variation is shown for two periods in Fig. 17 along with the predicted tidal heights and the day–night cycle. In the early part of the record each low tide is associated with an oxygen maximum, and the maximum which occurs during the day is larger than the one at night. Later in the month there has been a phase shift in the oxygen–tide correlation, with the oxygen maxima occurring during high tide, though the day-time maxima are slightly larger than the night-time maxima. Oxygen variations are also evident at frequencies higher than the semidiurnal tide. We suggest that these may reflect patchiness in the populations of photosynthetic and respiring organisms as the waters move through the measurement site with the tidal oscillation. To determine more exactly the processes associated with the various periods of oxygen variability will require information on the spatial scales of variations.

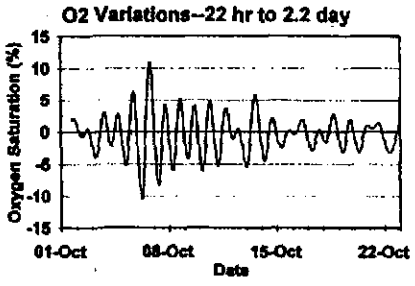

Fig. 16. The variation in oxygen saturation diel variations during three weeks in October 1993. The data in Fig. 13 were digitally filtered using a band pass filter that retains only those variations with periods in the range of 22 h to 2.2 days.

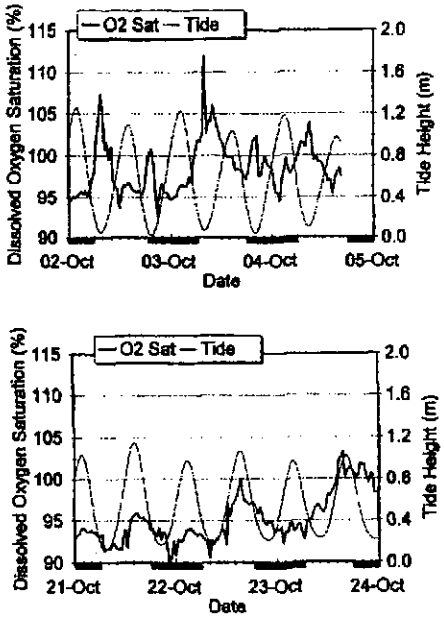

Fig. 17. Comparison of high-frequency oxygen variations with the tidal variation and the diel cycle. During the early part of the month each low tide is associated with an oxygen peak and the peak during daylight is larger in amplitude than the diurnal peak at night. During the later portion of the month the phase relation between oxygen and the tide have shifted.

This initial study of oxygen time-series in a coastal setting shows oxygen saturation variations on a large range of time scales. Measurement programs that employ seasonal, monthly, or weekly sampling cannot capture the variations that exist in biological, physical, and chemical properties.

6. Ocean color remote sensing

The final aspect of this study is an evaluation of the potential uses of ocean color satellite remote sensing in coastal waters. Perhaps in 1996 the SeaWiFS instrument will be launched by Orbital Sciences, Inc. which will provide a new generation of ocean color data to follow that which was available from 1978 to 1986 from the NASA CZCS (Coastal Zone Color Scanner) instrument. We have been examining

the historical CZCS data from the region off the northeastern U.S.A. to identify the spatial scales of variability of surface-water chlorophyll concentrations and to evaluate possibilities for combining in situ and remote sensing data in the future.

The CZCS instrument measured the light emitted by the ocean at five wavelength bands in the visible and near-infrared portion of the spectrum. NASA used a global algorithm to calculate surface-water chlorophyll (Chl) concentrations from the intensities of light at the different CZCS bands. The Chl concentrations are integrated values for the first optical depth of the water column (the depth to which visible radiation penetrates to within $1/e$ of the incident intensity). This depth depends on water clarity, and in this region it would be on the order of 5–25 m, or similar to the depth of the mixed layer during periods of seasonal stratification. We have worked with samples of both the 4-km and the 1-km horizontal resolution CZCS data. The 4-km images obtained during the spring of 1982 showed relatively high concentrations of chlorophyll. The contrast between shelf and slope waters and the Gulf Stream and a warm core ring off New Jersey was resolved clearly in the images. The maximum spatial resolution available from CZCS (and also expected from SeaWiFS) is 1 km by 1 km for each pixel. This resolution is especially valuable in near coastal studies which we have examined in the area off Rhode Island.

The scales of variability in the ocean color images of this region are in the range of 5–50 km. While it is sometimes possible to build a temporal time-series of ocean color satellite images, consistent temporal coverage is disrupted during periods of cloudiness. For quantitative use of the ocean color data more attention must be given to spatial variations in the atmospheric attenuation of the visible radiation, and to the separation of chlorophyll, suspended matter, and possibly blue-absorbing organic matter in the ocean color signal. The SeaWiFS sensor may be better able than the CZCS sensor to resolve these effects in coastal waters.

7. Summary

The results of this study demonstrate that variations in microconstituents among marine environmental compartments, whether defined in terms of chemical, physical, or biological factors, must be resolved on a range of time and space scales. Traditional sampling and measurements in coastal waters have generally under-sampled these scales of variability. Seasonal or monthly observations cannot resolve the large amplitude changes between compartments associated with diel, tidal, and meteorologically-driven processes. To adequately address the natural scales of variability in coastal waters will require the development and application of new technologies in marine chemistry. In situ measurement systems offer a promising approach. Satellite remote sensing, while not providing direct chemical measurements, can provide useful information about the some of the physical and biological processes in marine systems. Simple modeling approaches provide a means to link together diverse chemical, physical, and biological data sets with a knowledge of the major processes.

The box models provided useful insights into transports, residence times, and reactivities of oxygen and copper in Narragansett Bay. One assumption that is implicit in these models is that the salinity field in the estuary is in steady state with the freshwater inputs, the tidal exchange processes, and the estuarine circulation. This assumption will be valid when the freshwater flow, the tidal exchange, and any wind-induced circulation are relatively constant over periods of time comparable to the residence time of waters in the estuary.

Acknowledgements

This work was supported in part by Office Naval Research grant N000149410635 and by EPA Cooperative Agreement CR817743-01-2.

References

Bender, L.M., Kester, D.R., Cullen, D., Quinn, J.G., King, D.W., Phelps, D. and Hunt, C., 1989. Trace metals in the waters, sediments, and shellfish of Narragansett Bay. Rep. submitted to Rhode Island Dep. Environ. Manage., Narragansett Bay Proj., Providence, RI.

Dettmann, E.H., Brown, W.A., Warren, W.M., Fox, M.F. and

Kester, D.R., 1992. Final report on application of a wasteload allocation model to multiple discharge sources into an estuary. U.S. Environ. Prot. Agency, Environ. Res. Lab., Narragansett, RI, Contrib. No. 1381, 203 pp.

Doering, P.H., Weber, L., Warren, W.M., Hoffman, G., Schweitzer, K., Pilson, M.E.Q., Oviatt, C.A., Cullen, J.D. and Brown, C.W., 1988a. Monitoring of the Providence and Seekonk Rivers for trace metals and associated parameters. Data report: Spray cruises I, II, and III. Mar. Ecosystems Res. Lab., Univ. of Rhode Island, Kingston, RI, 359 pp.

Doering, P.H., Weber, L., Warren, W.M., Hoffman, G., Schweitzer, K., Pilson, M.E.Q., Oviatt, C.A., Cullen, J.D. and Brown, C.W., 1988b. Monitoring of the Providence and Seekonk Rivers for trace metals and associated parameters. Data report: Spray cruises IV, V, and VI. Mar. Ecosystems Res. Lab., Univ. of Rhode Island, Kingston, RI, 333 pp.

Doering, P.H., Oviatt, C.A., Weber, L.E., Welsh, B.L., Eller, E., Dettmann, E., Godshall, F. and Tracey, G.A., 1989. Characterizing late summer water quality in the Seekonk River, Providence River, and Upper Narragansett Bay. Rhode Island Dep. Environ. Manage., Narragansett Bay Proj., Fin. Rep.

Hansen, D.V. and Rattray, M., 1965. Gravitational circulation in straits and estuaries. J. Mar. Res., 23: 104–122.

Hansen, D.V. and Rattray, M., 1966. New dimensions in estuary classification. Limnol. Oceanogr., 11: 319–326.

Kester, D.R. and Magnuson, A., 1994. Evaluation of the YSI rapid-pulse dissolved oxygen sensor. Graduate School Oceanogr., Univ. of Rhode Island, Kingston, RI, Tech. Rep. No. 94-1, 22 pp.

Officer, C.B. and Kester, D.R., 1991. On estimating the nonadvective tidal exchanges and advective circulation exchanges in an estuary. Estuarine, Coastal, Shelf Sci., 32: 99–103.

Pilson, M.E.Q., 1985. On the residence time of water in Narragansett Bay. Estuaries, 8: 2–14.